1
Quantum Dot Technologies

Richard A. Hogg and Ziyang Zhang

1.1
Motivation for Development of Quantum Dots

The technologies that enable the creation of high-quality custom-engineered quantum dots (QDs) within a semiconductor matrix are of great importance for both new physics and new device applications. These "designer atoms," created either singly or as an ensemble within a device have already had a significant impact from the study of mesoscopic physics, and allowing the fundamentals of light–matter interaction to be probed, through to laser devices with new functionality. This chapter concentrates on the motivations, technological advances, and recent achievements of QDs applied to new light sources. Further chapters discuss the exploitation of such devices in a range of devices and applications. Here, we discuss the development of strained epitaxy to realize an ensemble of QDs for optoelectronic applications.

1.2
Gain and Quantum Confinement in a Semiconductor Laser

The semiconductor diode laser was first realized in 1962 by groups in The Soviet Union and the United States [1]. The acronym LASER (light amplification by stimulated emission of radiation), now assimilated into English as a word in its own right, indicates the unique characteristic of these devices, which harness stimulated emission, a process distinct from spontaneous emission, and absorption. In addition to the requirement for gain, feedback is also required to obtain lasing.

Figure 1.1a depicts these optical transitions schematically, along with their probabilities. Figure 1.1b depicts a situation where light is propagating through a semiconductor medium within a p–n junction, which is connected to a current source that modifies the carrier density in the active element. In the case of low current densities (low carrier density), absorption is the most likely process. Subsequent reemission of the photoexcited carrier will be in all directions, so the

The Physics and Engineering of Compact Quantum Dot-based Lasers for Biophotonics, First Edition.
Edited by Edik U. Rafailov.
© 2014 Wiley-VCH Verlag GmbH & Co. KGaA. Published 2014 by Wiley-VCH Verlag GmbH & Co. KGaA.

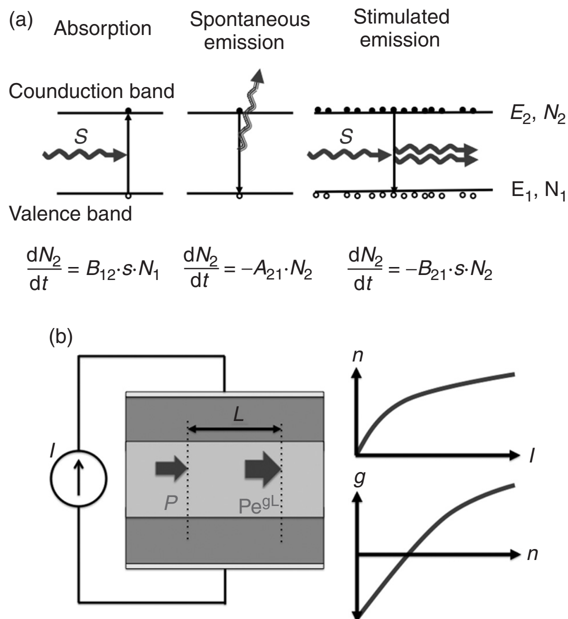

Figure 1.1 (a) Schematic of optical transitions between the conduction and valence bands in a semiconductor, including rates of these transitions. (b) Schematic of light propagating in a material where applied current modifies the carrier density, the rates of absorption, and stimulated emission, and hence gain.

propagating pulse will be denuded. As current (carrier) density is increased, the absorption rate is reduced and stimulated emission rates are increased. At some point in this lossless case, the rates of stimulated emission and absorption are equal and the material is transparent as $P_{out} = P_{in}$. In this ideal case, the transparency point coincides with population inversion, where there are an equal number of carriers in the upper state as there are in the lower state. As current (carrier) density is further increased, stimulated emission dominates and optical gain is obtained.

The density of electronic states at the lasing energy is of importance in determining the current densities required to achieve inversion, once the volume of the active element is defined. The magnitude of this gain is also a function of the radiative matrix element, and, in the case of high cavity powers, the rate at which carriers may be supplied. At first glance, a low density of states is attractive to minimize the threshold current of the laser. However, a real laser incorporates a lossy waveguide and facets. At least one of these facets should have moderate reflectivity to emit light, yet introduces further losses to the ideal system. Lasing is achieved when gain overcomes all losses. Therefore, a density of electronic states sufficient to provide gain to overcome these losses is a key requirement.

It is also important to remember that semiconductor materials form bands of states, so the kinetic energy of carriers, inhomogeneity of the material, and homogeneous broadening (e.g., carrier lifetime broadening due to free carriers

and phonon scattering) all act to broaden the gain spectrum. The characteristics of a particular material and heterostructure with regard to the effects of current and temperature on the gain spectrum are therefore of critical importance to the operation of a laser. These characteristics not only determine the static, but also the dynamic performance of the laser diode. In addition to the characteristics of the semiconductor material, the dimensionality of the charge carriers in a system determines the form of the density of electronic states.

Figure 1.2 shows a schematic of the density of states as a function of dimensionality, going from bulk (3D) to QD (0D) systems. The move to a quantum well (QW) structure removes a kinetic energy component from one spatial direction from the total energy of the carrier, replacing it with a quantum confinement energy. This step-like density of states is beneficial as the radiative rate is enhanced as compared to the bulk material, and carriers are concentrated at a specific wavelength. For bulk materials, the joint density of states (the product of electron and hole densities of state) is very low at the band gap, yet these states must be filled in order to access energies where gain may be sufficient to overcome cavity losses. The carriers used to fill these states are essentially wasted. A simple, yet nontrivial advantage of a QW active element over bulk is the reduction in volume, which goes hand-in-hand with a reduction in drive current. This (along with more efficient use of carriers) ameliorates many problems for semiconductor lasers associated with large currents and finite resistance, resulting in large joule heating effects.

As we move to the QD system, there is no free motion in any direction, and an atom-like delta function is obtained for the density of states. This atom-like character allows many new aspects of physics to be explored. With regard to semiconductor lasers, 0D systems have a number of predicted advantages. Arguably, a key motivator for the development of technologies to realize QD materials was the prediction of a temperature-insensitive threshold current by Arakawa and Sakaki in 1982 [2]. They explained that this would be achieved if only the ground sub-bands

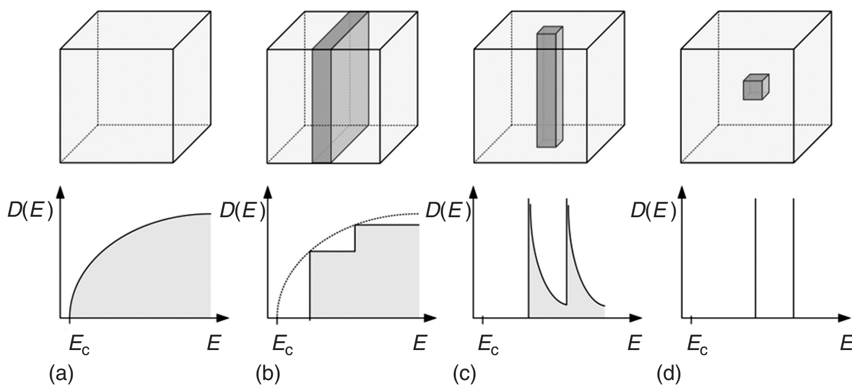

Figure 1.2 Schematic of effect of electronic confinement on the density of states moving from (a) bulk to (b) one-dimensional confinement in a quantum well, (c) two-dimensional confinement in a quantum wire, and (d) three-dimensional confinement in a quantum dot.

were populated (i.e., the state separation was large compared to $k_B T$, where k_B is the Boltzmann coefficient and T is the absolute temperature). This is possible by choosing sufficiently small dimensions for their ‘‘3D-quantum well’’ (prior to the adoption of the term *dot* for 3D confinement/0D carrier systems). In 1986, Asada *et al*. [3] modeled the electronic dipole for different carrier dimensionality and showed an increase in material gain for a ‘‘quantum box’’ (again, prior to the adoption of ‘‘dot’’ for 0D systems).

While these two reports are not the only theoretical predictions of the benefits of a QD active, they are certainly very compelling. The temperature sensitivity of a semiconductor laser is a major issue in their deployment in real-world applications. In optical communications, there are typically maximum launch power limits, and minimum receiver powers required to achieve efficient data transmission. As such, large variations of the laser power cannot be tolerated. In fact, the temperature sensitivity of lasers can be so large that they simply cannot be operated at two biases (logic level 0 and 1) over the whole temperature range. This temperature sensitivity results in the need for temperature monitoring and control, resulting in large packaging costs for laser modules as this tends to be rather labor intensive. Secondly, an enhanced gain at low current densities has clear advantages in terms of energy consumption, where very low currents also translate to low self-heating. This high gain for low current characteristic is also of importance in the dynamic performance of the laser, where differential gain plays a key role in direct modulation rates, and the differential gain spectrum dictates the change in lasing wavelength during modulation (chirp) [4].

As a consequence of major advantages such as these, there has been a great deal of work focused on the practical realization of such devices. The challenge of this task is not to be underestimated, as we require many factors to be simultaneously realized in our ideal QD laser active. We require the creation of structures with dimensions off ~10 nm per side (~30 atoms per side) in order to have good carrier confinement in all three dimensions. These QDs must be inserted within a semiconductor matrix, minimizing the formation of crystal defects as this will not only act as carrier recombination centers but may also pose problems for device reliability and commercial exploitation of the technology. Another major challenge is that in order to harness all the predicted benefits of QDs in a laser device, all QDs should be essentially identical [5]. The QDs required consist of ~27 000 atoms embedded in a crystal matrix, with an ensemble of these differing in emission energy by only a few millielectron volts.

1.2.1 Top-Down Approach

An obvious route to realize QDs is to create a QW and etch ~10 nm scale features. Here high-resolution lithography (e.g., electron beam lithography) is followed by well-controlled etching. Dry etching is a popular method owing to the high uniformity and accurate control of etch depth. However, dry etching brings with it significant issues as the process induces damage to the nanometer scale features.

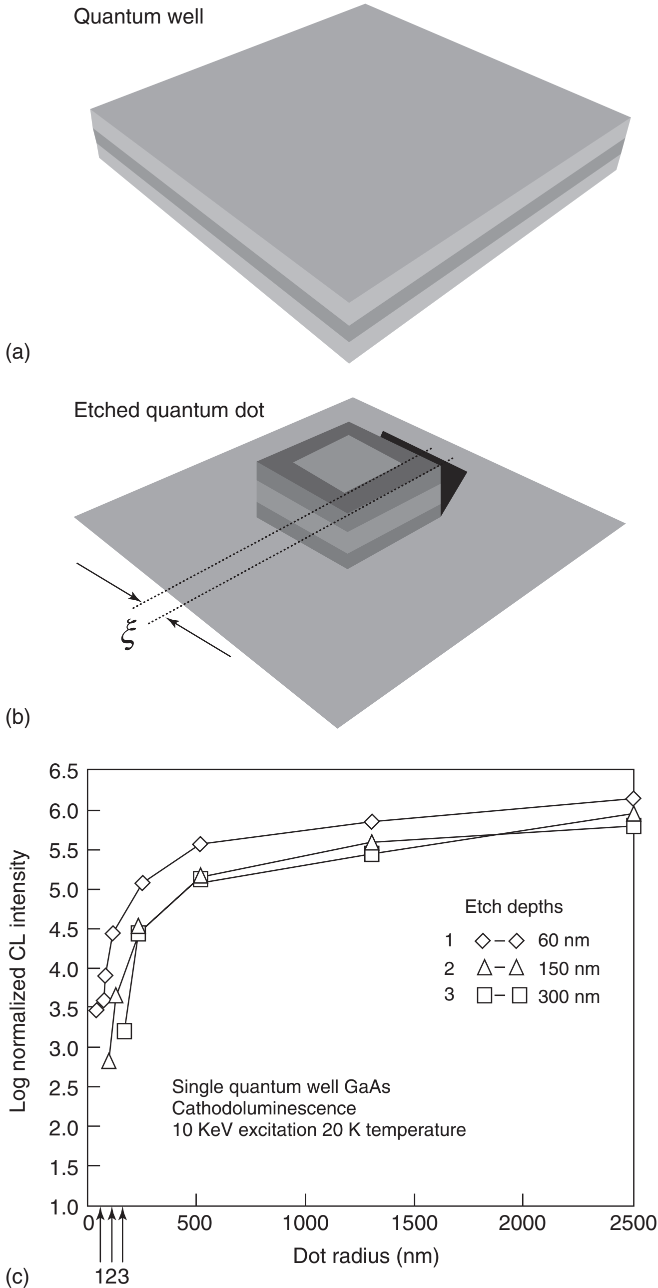

Figure 1.3 (a–b) Schematic showing the creation of a damaged, optically dead layer when creating a quantum dot through etching of a quantum dot. (c) graph shows CL intensity of etched structures as a function of dot radius. Arrows indicate points at which the quantum dot was optically dead, providing an estimate of ξ, the thickness of damaged material introduced by the fabrication process. (Source: Clausen *et al*. 1989 [6]. Reproduced with permission of Appl. Phys. Lett.)

This was highlighted by Clausen *et al*. [6], who characterized dry etched structures by low temperature cathodoluminescence (CL). They found a significant reduction in luminescence (see Figure 1.3) as the etched structure diameter was reduced, with the data only being explained by the presence of a damaged layer of finite thickness. The arrows in Figure 1.3 indicate the point at which no luminescence was observed from their QD structures, and provides an estimate for the thickness of this damaged layer. Layer thickness of 90–200 nm were deduced, significantly larger than the scale of features required to achieve good electronic confinement in all three dimensions. This finite thickness precludes the use of postetch passivation treatments, and poses a key technological barrier for this route of manufacture for QDs.

In addition to overcoming etch-induced damage, surface recombination and the need for the incorporation of the QDs within a p-i-n diode require the regrowth of any etched features, their planarization, and the formation of a waveguide/doped upper layers. Significant effort has been spent in this direction, with QD lasers being realized in the InP/InGaAsP system [7]. Figure 1.4 shows a schematic of their structure. Here, electron beam lithography was combined with wet etching. In order to maintain etch anisotropy, the uppermost layer was InGaAs, which was subsequently removed by selective wet etching prior to regrowth of the structure as a buried heterostructure laser. The laser operated at 77 K with emission from QD excited states because of limited ground-state gain at a current density of

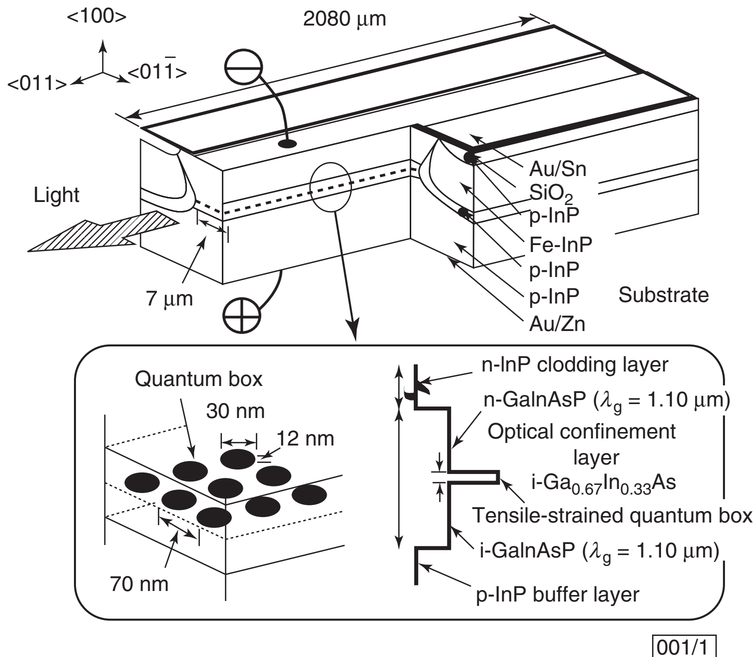

Figure 1.4 Schematic of an etched and regrown quantum dot laser. (Source: Hirayama *et al*. 1994 [7]. Reproduced with permission of Electron. Lett.)

7.6 kA cm^{-2}. This is the best laser performance reported for devices utilizing an etch to a QW structure.

1.2.2 Bottom-Up Approach

An alternative method for QD manufacture is to rely on preexisting patterning of the semiconductor substrate followed by epitaxy, which is modulated by the existing pattern [8]. Figure 1.5 shows the fabrication process in further detail. Upon a GaAs substrate, a dielectric layer is deposited. This dielectric layer is patterned through electron beam lithography and dry etching. Following cleaning of the wafer (a combination of oxygen plasma and wet etching), the wafer is loaded into the epitaxial growth reactor (in this case metal-organic vapor phase epitaxy (MOVPE)) for the deposition of GaAs. The presence of the dielectric mask allows the deposition of semiconductor only within the etched gaps and modifies the supply of materials owing to a change in the density of reagents in the gas phase [9]. Owing to the symmetry of the crystal structure and control of the epitaxial growth parameters, a pyramid-like structure is formed, which then coalesces, resulting in the formation of pyramid-shaped indentations in the GaAs. Here, the subsequent deposition of a QW upon the 3D structure is modified, leading to the formation of QD-like structures, confirmed by spatially resolved luminescence measurements.

This technique has not resulted in practical laser devices for several reasons. The dielectric materials buried by the epitaxial materials present difficulties in forming a low loss waveguide structure. Furthermore, the QDs that are formed are strongly

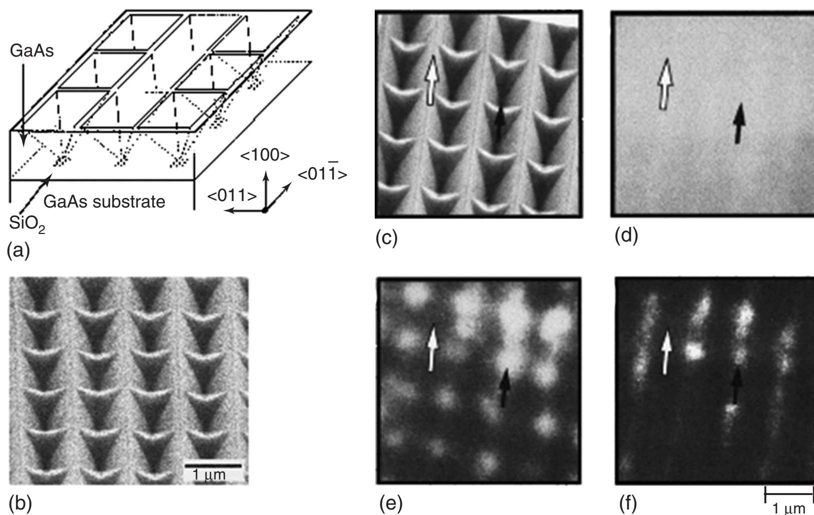

Figure 1.5 (a–f) Schematic of a patterned and MOVPE regrown structure and cathodoluminescence imaging of the quantum dot emission. (Source: Ishida *et al.* 1998 [8]. Reproduced with permission of Appl. Phys. Lett.)

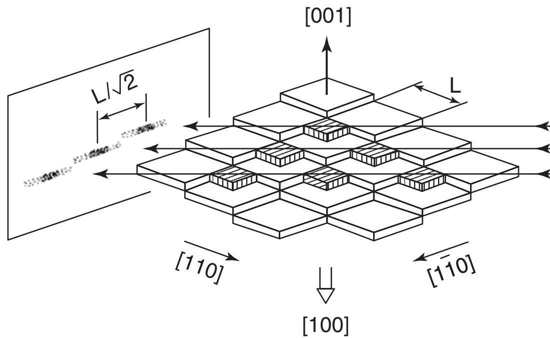

Figure 1.6 Schematic of terraces upon the substrate surface utilized to form submonolayer quantum dot structures. (Source: Brandt *et al*. 1991 [10]. Reproduced with permission of Phys. Rev. B.)

coupled to QW layers in the structure, and have poor electronic confinement. A serious impediment to application is the low areal QD density that can be achieved. With one QD per 1 μm × 1 μm, an areal density of QDs of 10^8 cm^{-2} is achieved. A very low density of states and concomitant low maximum gain would result.

An alternative approach was demonstrated by Brandt *et al*. [10], where the growth of monolayer InAs islands (and their subsequent encapsulation with GaAs) was achieved. This was made possible by the presence of well-defined step structures on the crystal surface, achieved by careful control of the growth of GaAs by step propagation. A suitably misoriented substrate (see Figure 1.6) then favors the formation of InAs islands at these step edges through submonolayer deposition. Spectroscopy of these structures indicated QD-like behavior, but owing to the small height of these structures (one monolayer), the barrier to electronic escape was quite small, limiting their possible use to very low temperatures. However, such structures point the way to the use of self-assembly techniques to realize QD materials for optoelectronic devices.

1.3 Self-Assembled Quantum Dot Technology

1.3.1 Molecular Beam Epitaxy

Compared to the QD fabrication technologies described above, self-assembled QD technologies are a more effective and popular technique to achieve high quality, dislocation-free QDs. Through almost 30 years of study, the self-assembled QD growth technique has already become a mature technology. Today, many QD devices have been commercialized including lasers, broadband light emitters, and passive devices [11], which are all based on self-assembled QD structures. Here, we describe the main growth technique, the growth dynamic processes, and the thermodynamic processes at play in the growth of self-assembled QDs.

The molecular beam epitaxy (MBE) growth technique is a state-of-the-art thin film epitaxial growth technique. MBE technology was invented in 1968 by Arthur Cho from Bell Laboratories. By 1971, Cho and Arthur [12] had developed it into a mature ultrathin layer material epitaxy growth technology. MBE is carried out under high vacuum, with different groups of atoms being provided a high thermal velocity, forming a molecular beam that is incident upon a heated substrate surface.

MBE has many advantages compared with other epitaxial growth techniques such as liquid phase epitaxy (LPE), vapor phase epitaxy (VPE), and MOVPE [12] such as

1) low substrate temperatures which can reduce the diffusion of impurities to obtain a steep impurity distribution of the epitaxial layers;
2) very low growth rate leading to precise (atomic level) control of doping, composition, and thickness of the epitaxial layers;
3) MBE growth is a dynamic process, that is, it is not carried out under conditions of thermal equilibrium, allowing the growth of materials that cannot be obtained by heat balance;
4) owing to the high vacuum, the growth process and the surface of the sample can be analyzed and monitored *in situ*.

Compared with the other ultrathin film growth technique (e.g., MOVPE), these differences (disconnect of material supply rate and substrate temperature, *in situ* monitors, etc.) allow for higher quality QD device structures through MBE. While for InP-based QWs MOVPE technologies dominate, all current commercial activities in the field of GaAs-based QDs are MBE based.

Figure 1.7a is a photograph of a VG 90 MBE reactor [13], which is constituted by three main parts – preparation chamber, transfer chamber, and growth chamber. These three chambers have vacuum valve isolation, and therefore samples can be freely transferred among the three chambers while maintaining high vacuum conditions. As seen in Figure 1.7b, in the growth chamber, molecular source ovens are placed opposite the substrate. The MBE epitaxial growth takes place in an ultra-high vacuum ($<10^{-10}$ Torr), and may form various compound semiconductor materials (e.g., InAs, InSb, and GaAs). Once the distance between the source oven and substrate is fixed, the growth rate is mainly determined by the temperature of the oven.

Reflection high-energy electron diffraction (RHEED) is an important *in situ* analytical instrument in MBE, which is used in a number of ways. Firstly, it can be used to more accurately determine the temperature of the substrate (than pyrometry and thermocouples) via the observation of the transition from an amorphous image to a streaky RHEED pattern when the native surface oxide layer is removed from the sample. Secondly, the oscillation of the RHEED pattern is periodic with the formation of individual monolayers upon the substrate. As a consequence, it may be used to measure the growth rate. Thirdly, the RHEED pattern can be used to identify the formation of the QDs. Typically, the RHEED pattern for two-dimensional growth (i.e., layer by layer) shows a stripe pattern. The change of this pattern to a discontinuous line or ‘‘spotty’’ corresponds to the transformation of growth to a three-dimensional process.

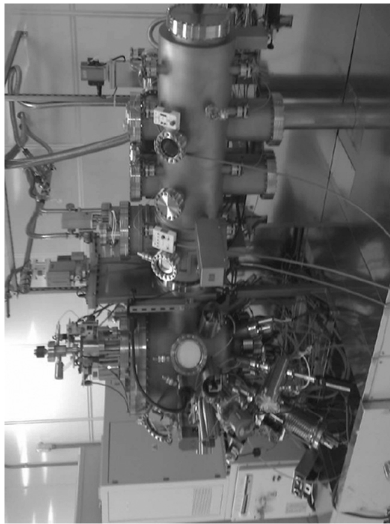

(a)

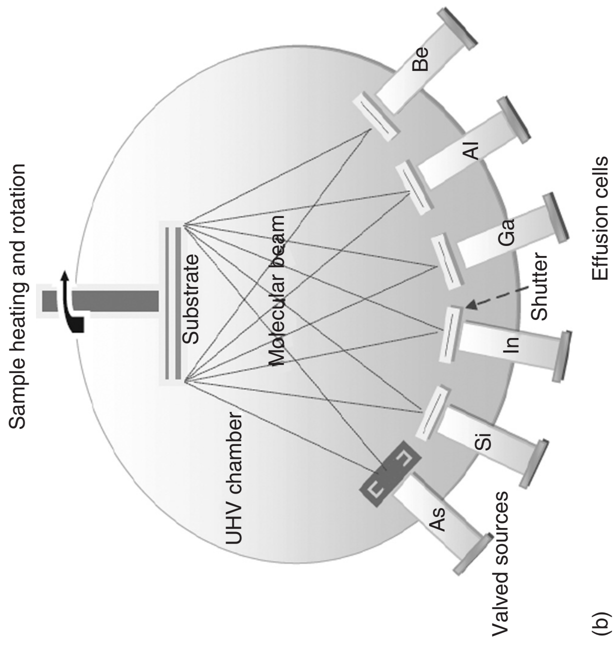

(b)

Figure 1.7 (a) Photograph of a VG 90 MBE reactor and (b) schematic of the MBE growth chamber and growth process.

1.3.2 Growth Modes

Generally, there are three main MBE heteroepitaxial growth modes that are dictated by the lattice mismatch, the surface energy, and the interfacial energy. The Frank–van der Merwe (FM) growth mode is a layer-by-layer growth mode routinely utilized in the growth of QW structures. Here ad-atoms attach preferentially to surface sites. In the Volmer–Weber (VW) growth mode ad-atom/ad-atom interactions are strong and clusters of ad-atoms are formed upon the surface. The Stranski–Krastanow (S–K) growth mode is a hybrid of FM and VW growth modes.

If the lattice mismatch is small and the surface energy of the epitaxial layer and the interfacial energy is less than the surface energy of the substrate, the epitaxial growth mode will be FM mode. If the lattice mismatch is large and the surface energy of epitaxial layer is greater than the surface energy of the substrate, the epitaxial growth will be through the VW mode. For moderate lattice mismatch, as shown in Figure 1.8, the initial growth is layer by layer, and strain due to the lattice mismatch is accumulated with increasing thickness of the epilayer. When the thickness of the 2D layer reaches a critical level, the strain will be released by the formation of small islands. As epitaxial material is added, these small islands will continue to grow until fully ripened. This process characterizes the hybrid S–K growth mode.

This growth technique is now widely used to achieve dislocation-free QD materials, which are termed *self-organized* or *self-assembled* QDs. The initial 2D layer is called a *wetting layer*, and the QDs include both the islands and the wetting layer. The critical thickness, the transition from 2D to 3D growth, the size of the islands, and the areal density of dots is generally related to the lattice mismatch between substrate and deposited layers and the growth conditions (substrate temperature, the V/III beam ratio, growth rate, etc.). In the following, we describe from kinetics and thermodynamic effects to the self-organized QD growth mechanism for InAs QDs on a GaAs substrate. The impact of several important factors upon the growth process is outlined.

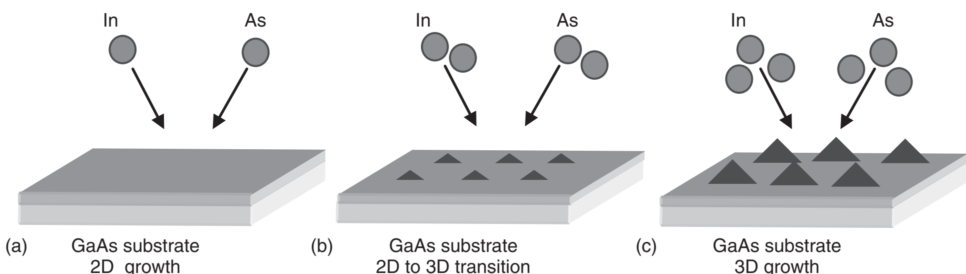

Figure 1.8 (a–c) Schematic of the three main stages of self-assembled quantum dot formations under the S–K growth mode.

1.3.3 Quantum Dot Growth Dynamics

The QD growth process is far from equilibrium, so aspects of the dynamic processes are very important to determine the film morphology. Growth kinetics processes (depicted in Figure 1.9) mainly consist of adsorption, surface migration, nucleation, diffusion to the substrate (intermixing), step incorporation, and island incorporation. Kinetic processes depend mainly on two factors. Firstly, surface conditions including the orientation of the substrate, morphology of the surface, stress distribution, and any compositional gradient across the surface of the substrate. These factors mainly refer to the state of the substrate surface before QD epitaxial growth.

Secondly, the surface density of the adsorbed atoms and their diffusion is another critical factor. The density and diffusion of the adsorbed atoms can be controlled by changing the growth conditions such as the deposition rate (cell temperatures) and the substrate temperature. This process is relatively complicated and is a major factor in the control of the epitaxial growth of QDs. There are several key factors that can affect the actual QD growth process.

1.3.3.1 The Interaction of the Quantum Dot and the Wetting Layer

The wetting layer and QDs are closely related. There are different views on their connection and interplay within the literature. It has been proposed that the thickness of the wetting layer is exactly the critical thickness, and QDs are grown on the complete wetting layer. However, there are other reports that propose that after the formation of the QDs the wetting layer is destroyed and that the wetting layer epitaxial materials are also involved in the formation of the QDs. Our view supports the latter theory. Gerard *et al.* [14] used different growth methods (e.g., inclined substrates) to study different InAs layer thickness and their corresponding photoluminescence (PL) characteristics, and found that when the QD light-emitting intensity increased, the wetting layer luminescence sharply decreased. Many theoretical models [15, 16] indicate that the 2D–3D growth mode transition is a phase transition. The beginning of the phase transition is the wetting layer, and these transitions end with the formation of stable island structures. This means that the formation of the QDs may only require the consumption of the wetting layer without the further deposition of epitaxial material.

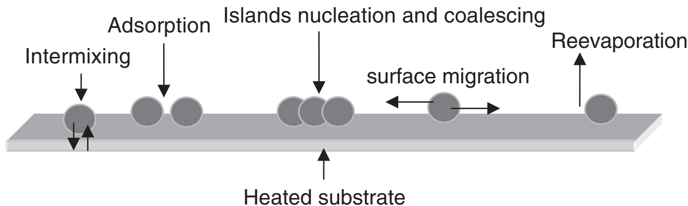

Figure 1.9 Schematics of growth dynamics, including adsorption, nucleation, migration, reevaporation, and intermixing.

1.3.3.2 **The Interaction of the Quantum Dot with Underlying Layers and Capping Layers**

Many experiments have demonstrated that the indium composition in the fully encapsulated QDs is not uniformly distributed, with the indium composition reducing with increasing distance from the center of the QD. The InAs QD, realized by S–K growth and overgrowth, is therefore a nucleus of high indium composition alloy [17]. If it is assumed that the QD is of a triangle shape, then the bottom of the island is the large strain area, and at the top of the island the strain is relatively small. Therefore, when the QD is buried, the InAlAs or InGaAs capping layer will accumulate more at the top of the island than at the bottom. From this perspective, the introduction of the burying layer can effectively maintain the morphology of the QDs. In addition, the growth temperature of the QDs is generally above 480 °C; in this case, indium–gallium intermixing is significant, which will lead to a large modification of the indium composition, and hence, the shape of the QD. Before entirely covering the QDs with a GaAs layer, the insertion of layers with appropriate fractions of InAlAs or InGaAs will partially weaken the stress in the QDs, and hence inhibit the degree of indium–gallium intermixing. As a result, InAlAs or InGaAs covering layers are usually used to extend the emission wavelength of QDs to longer wavelengths. The InGaAs strain reducing layer [18] modifies the pure InAs/GaAs QDs into InGaAs/GaAs QD structures via atomic interdiffusion between indium and gallium. This interdiffusion is more obvious when using an InAlAs capping layer or underlying AlAs layer. Meng *et al.* [19] found that if the InAs QDs are grown on an AlAs layer (instead of a GaAs layer), the InAs wetting layer will be completely consumed because of the strong atom interdiffusion between indium and aluminum, as seen in Figure 1.10.

1.3.3.3 **Growth Interruption**

During the QD epitaxial growth, growth interruption has a significant impact on the morphology of the QDs. Ledentsov *et al.* [20] carried out a systematic study of the effects of growth pause on InAs/GaAs QDs. Usually during QD growth, a short pause will provide sufficient time for indium atoms to migrate

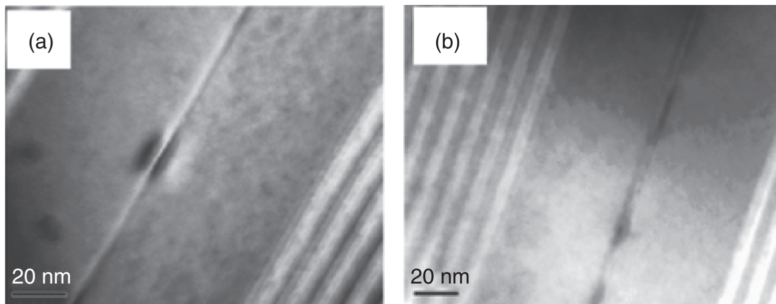

Figure 1.10 Cross-sectional TEM images of InAs QDs (a) grown on 8 ML AlAs and (b) grown on 2 ML AlAs. (Source: Meng *et al.* 2010 [19]. Reproduced and modified with permission of J. Appl. Phys.)

on the sample surface to find optimal positions for incorporation, which could be beneficial to obtain uniform dot size (and composition) distribution. Different substrate temperatures, different arsenic pressure, and different InAs deposition amounts require different growth interruption times to allow the QDs to achieve an equilibrium dot size. For example, maintaining the substrate temperature at 480 °C, arsenic pressure of $<2 \times 10^{-6}$ Torr and 3 Monolayer (ML) InAs deposition amount, a 10 s growth interruption is required to lead to the majority of the QDs to reach 14 nm transverse width (the equilibrium dot size). For the deposition of 2.5 ML InAs to form the QDs, with the same growth conditions, a 40 s growth interruption is required, while for 2 ML InAs, a growth interruption of 100 s is needed to achieve the same results as above. However, when the lateral size of the QDs has reached 14 nm, with further increase in the growth interruption time, the QD size and morphology will no longer change [21].

This is a dot size self-limiting effect. During the growth interruption, the smaller QDs will grow to be bigger, and the large dot will lose material and become smaller, and finally all the QDs have a tendency to be of the same average size. The above discussion assumes no desorption of atoms during the growth interruption. However, in the actual process of the QD growth, the growth temperature is generally higher than 480 °C, so that atomic desorption is always a factor that should be considered. However, a suitable growth interruption has a great impact on the size, uniformity, and shape of the QDs.

1.3.3.4 **Arsenic Pressure**

Arsenic pressure is one of the most important factors in the formation of InAs QDs. Varying the arsenic pressure will affect the surface energy and cause changes in the surface structure of the GaAs substrate. An appropriate arsenic pressure reduces the accumulation of surface clusters. An excessive As pressure will result in the formation of clusters in large areas of the substrate surface, while too low an arsenic pressure is not conducive to the 2D–3D transformation. In the InAs/GaAs QD system, arsenic pressure can affect the level of migration of indium atoms on the growth surface. Low As pressure will lead to a higher mobility of the indium atoms, and thus will lead to larger dot size and lower areal density distribution of the QDs. Conversely, large arsenic pressure leads to low mobility of the indium atoms, and small dot size and high density of the QDs. Yamaguchi *et al*. [22] have used a very low arsenic pressure ($<6 \times 10^{-7}$ Torr) and utilized a low growth rate to obtain uniform (composition and size) QDs (PL linewidth of 18.6 meV at 14 K).

1.3.3.5 **Growth Temperature**

A very effective method to extend the emission wavelength of InAs/GaAs QDs to 1.3 μm or beyond is by raising the growth temperature of the substrate. For 1.3 μm QD materials, a typical substrate temperature of above 500 °C is used. Besides achieving long-wavelength emission from the QDs, high substrate temperatures are also employed for short-wavelength QD materials (e.g., red InAlAs/AlGaAs [23]). In this kind of QD structure, the aluminum composition is very high, which is usually disadvantageous for the growth of high-quality QD laser structures because the high aluminum composition will readily incorporate oxygen and other impurities

into the InAlAs QD structures. In addition, the high aluminum composition will tend to increase the density of group III vacancies during QD growth. Therefore, an appropriately high growth temperature will increase the migration length of aluminum atoms, thereby reducing the incorporation of unwanted/undesirable species and group III vacancies. Chu *et al.* [24] have systematically studied the influence of the substrate temperature on the growth process of InAs/GaAs QDs. They found that when the temperature was changed from 480 to 530 °C, the dot size increased along with a decrease in the dot density, as seen in Figure 1.11.

1.3.3.6 Growth Rate and Material Coverage

During the epitaxy growth of QDs, the optimization of growth rate and the material coverage to form the QDs is also essential. A low growth rate leads to a highly uniform QD size/composition distribution, which is a quite similar effect to the use of a growth interruption. For long-wavelength QD devices, we require large QDs, which will consume a large amount of deposited materials. However, an excess of deposited materials will introduce misfit dislocations and other defects.

It is noteworthy that the growth parameters described above are mutually interdependent, and some of them have similar effects on the QD growth. For example, low growth temperature and high As pressure have similar effects, as do long growth interruption and low growth rates.

1.3.4 Quantum Dot Growth Thermodynamic Processes

The study of the kinetic processes for QD growth is critical, but a thermodynamic study is also necessary because under high growth temperature and low growth rate conditions, the surface ad-atoms have enough time to migrate to their energy-balanced location, making the system close to thermodynamic equilibrium.

As seen in Figure 1.12, there are three main stages for the QD S–K growth mode. These are Phase A, corresponding to 2D growth; Phase B, the 2D–3D transition; and Phase C, corresponding to QD ripening [25]. In Phase A, at the initial stage

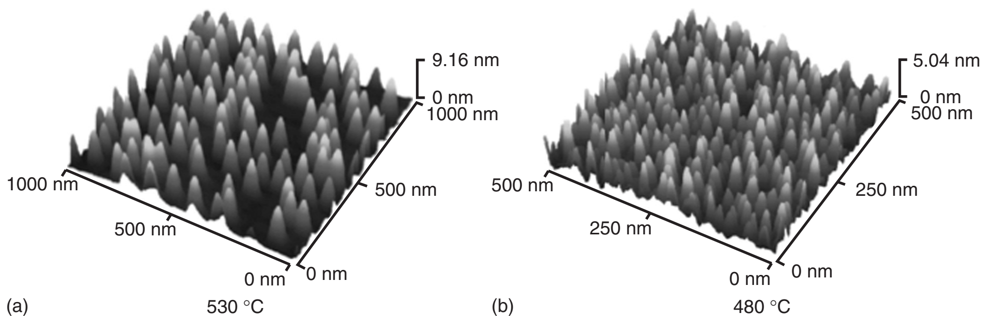

Figure 1.11 (a,b) AFM images showing the effect of growth temperature on quantum dot areal density and size. (Source: Chu *et al.* 1999 [24]. Reproduced and modified with permission of J. Appl. Phys.)

of material deposition, the epitaxial growth will follow the 2D growth mechanism, resulting in the epitaxial layer being incorporated into the substrate. The strain is accumulated with increase in the thickness of the 2D layer. When the deposition time reaches t_{cw}, 2D growth is no longer stable, and the 2D metastable growth begins.

Phase B can be divided into two steps: nucleation and growth. For nucleation, at point X, the excess strain energy in the 2D layer will be released by the 2D–3D transformation. The surface density of the QDs is determined by the concentration of nucleation points. When the stress field generated by the different QDs on the substrate begins to overlap with each other, a dense arrangement of the QDs will be formed. There will be a subsequent 3D island growth process, along the surface of the wetting layer and 3D islands, where the strain energy distribution is uneven. The changes in strain energy density will affect the surface materials and modify the chemical potentials.

With the formation of the islands, there is a local change in the strain. At the edges of the islands, strain is high, while on the top of the islands, strain is reduced. The atoms deposited on the surface of the wetting layer must overcome the potential energy barrier at the edge of the island to be incorporated into the island. The chemical potential around the 3D islands is related to the size of the islands [26]; the larger the island, the higher the energy barrier. As long as the surface of the wetting layer has a new atom absorbed, and adherent to the islands, the energy barriers of the islands will increase, which then increases the difficulty for further capture atoms. This has a size self-limiting effect on the QDs. We have described similar processes in the dynamics process of the QDs. Stage C corresponds to ripening (between point Y and the point Z in Figure 1.12). The decrease in the total energy of the QD system is not obvious. At this stage, the migrating atoms have

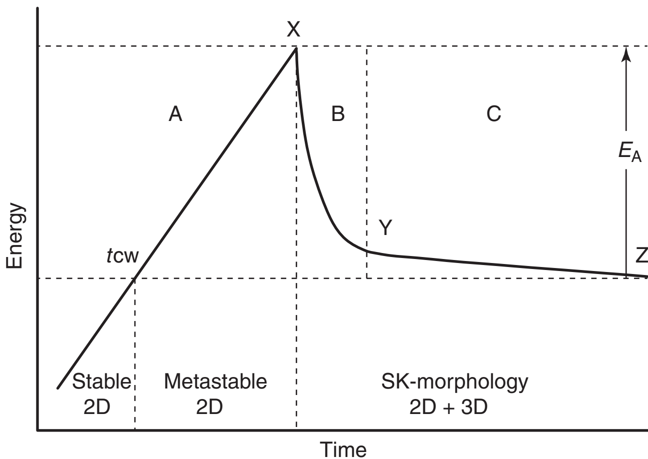

Figure 1.12 Schematic showing phase transitions in thermodynamic model for the formation of self-assembled quantum dots. (Source: Seifert *et al*. 1997 [25]. Reproduced and modified with permission of J. Crystal Growth.)

been exhausted. However, there are still some slow interactions (e.g., diffusion of the materials on the surface) among different dots due to different dot sizes causing different chemical potentials. Finally, the system will reach equilibrium.

1.4 Physics and Device Properties of S–K Quantum Dots

1.4.1 Temperature Insensitivity

The predicted temperature insensitivity of QD lasers was rather illusive. Early InAs/GaAs devices demonstrated performance similar to conventional QW devices [27]. In order to achieve very low temperature sensitivity, modulation p-doping of the active region has been employed [28, 29]. The initial prediction of temperature-

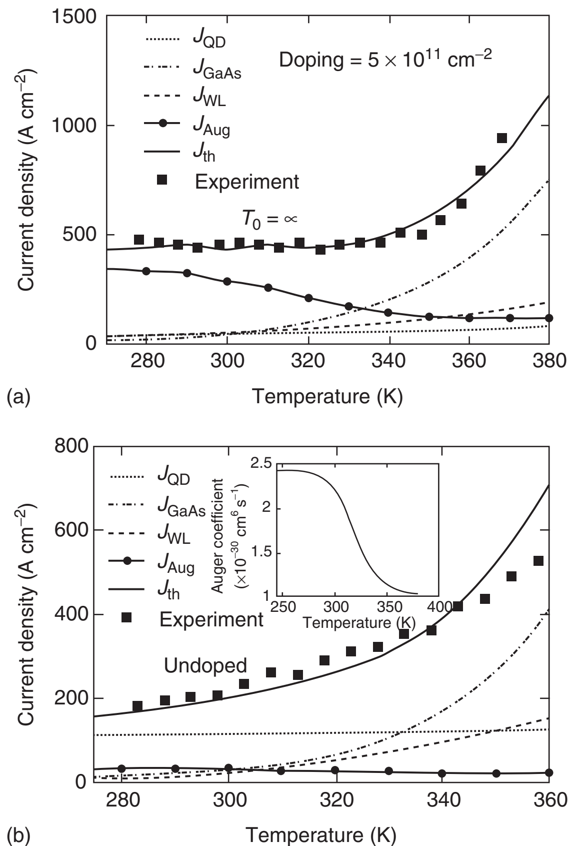

Figure 1.13 Effect of modulation p-doping (a) on realizing threshold current temperature insensitivity as compared to an undoped control sample (b). (Source: Fathpour *et al*. 2004 [29]. Reproduced with permission of Appl. Phys. Lett.)

insensitive emission [2] was dependent upon the inter sub-band state separation being much larger than k_BT. This is not true for the high effective mass hole states, and modulation p-doping of the active was proposed to completely fill these states. Figure 1.13 reproduces data from Fathpour *et al.* showing the effect of modulation p-doping on the threshold current density. Both an increase in the absolute value and an insensitivity to temperature are observed. While modulation p-doping is successful in achieving temperature insensitivity, with many groups having employed this technique, the precise mechanism(s) at play is the subject of considerable debate within the literature [30].

1.4.2
Low Threshold Current Density

Owing to a reduction in the density of states, brought about by a reduction in the active volume, there is an expected reduction in threshold current density for QD lasers. Figure 1.14 plots a historical review of the threshold current density of various types of semiconductor heterostructure [31]. The graph contains a large number of combined effects. It paints a picture of the double heterostructure (DHS) being initially introduced and reducing threshold current density, followed by the first QW laser, which was initially of very high threshold current density, and took ~10 years of development in terms of crystal growth, device fabrication, physical understanding, and device design to achieve its full potential. A similar story is also seen for self-assembled QDs where control of the S–K growth mode and optimization of the growth for a laser structure resulted in a 100-fold reduction in threshold current density over a few years.

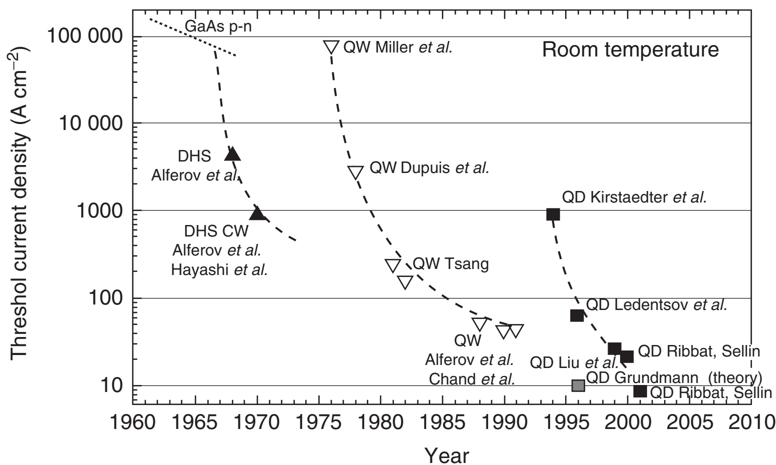

Figure 1.14 Plot of record threshold current densities for various types of semiconductor laser heterostructure with publication year. (Source: Bimberg 2005 [31]. Reproduced with permission of J. Phys. D: Appl. Phys.)

1.4.3 Material Gain and Modal Gain

While the threshold current density is a good indicator of material quality providing a handle on key parameters such as carrier lifetime and internal loss, it is not a perfect figure of merit for the laser. The modal gain, and its rate of change with carrier density (differential), is rather more critical. For high modal gains, a high mirror loss can be tolerated in a Fabry–Perot laser, which in turn leads to higher slope efficiencies. A high differential gain is of importance in high-speed modulation of the laser for applications such as data communications.

Initial measurements on QD lasers indicated very high values for the material gain of $\sim 6 \times 10^4\,\text{cm}^{-1}$ [32]. However, while the material gain is high, the overlap of the optical mode with the active element is small both due to the small height of the QDs (∼8 nm) compared to the optical mode (∼300 nm) and due to the small areal coverage (∼10%) of the plane of QDs. A further issue is the inhomogeneity of the self-assembly process, which introduces a variation in the size and composition of each QD. This inhomogeneous broadening of the ensemble of QDs is a major issue in obtaining high peak gains. As such, the modal gain of QD lasers is quite modest with typical values of $\sim 3\,\text{cm}^{-1}$ per QD layer [33]. Work to maximize areal density and minimize the inhomogeneous linewidth has produced lasers operating at the technologically important 1300 nm wavelength with gains of $\sim 7\,\text{cm}^{-1}$ per QD layer [34]. The comparative size of the inhomogeneous and homogeneous linewidth also plays a critical role in determining the lasing spectrum [35], and has been predicted to play a role in the temperature sensitivity of QD lasers.

Figure 1.15a shows a plan-view transmission electron microscopy (TEM) image of QD materials with emission wavelengths in the 1200–1300 nm region. Here, the random positioning of the QDs is apparent, as is the low fill factor of QDs within the sheet of QDs. This small value again acts to limit the modal gain, while the material gain is higher than that for bulk or QW materials. In order to ameliorate this, multiple layers of QDs are employed, as shown in Figure 1.15b. However, owing to issues with strain coupling between QD layers, which modifies the epitaxy of subsequent layers, multiple layers of QDs may not be placed as close together as is the case for multiple QW active elements.

1.4.4 Broad Spectral Bandwidth Devices and Spectral Coverage

For many applications of semiconductor lasers, a narrow laser emission is required. This is particularly true in fiber-optic communications where chromatic dispersion may be the limiting factor in transmission link lengths. However, for some applications devices with broad emission and/or gain spectra are highly desirable. The drive to reduce component inventory pushes semiconductor optical amplifier (SOA) manufacturers to make ever-broader spectral bandwidth devices covering one or more of the optical communication bands. Similarly, tunable laser components may differentiate themselves from other products through their spectral coverage.

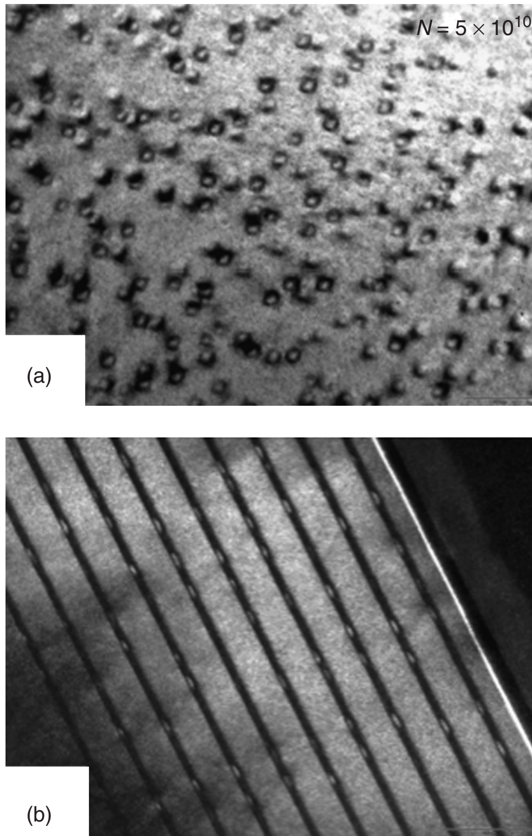

Figure 1.15 (a) Plan-view dark-field TEM image of a layer of quantum dots indicating areal densities of $5 \times 10\,cm^{-2}$. (b) (200) Dark-field cross-section image of a 10 layer quantum dot laser device (Courtesy of Igor Krestinov, Innolume GmbH).

Mode-locked lasers find application in various biophotonic applications such as laser surgery and multiphoton imaging. An important factor in determining their suitability is the pulse duration, which is inversely proportional to the gain spectral bandwidth [36]. A short pulse width is critical for producing high instantaneous powers needed for these nonlinear processes. For biomedical imaging applications such as optical coherence tomography (OCT), the spectral linewidth directly relates to the axial resolution [37] with ~100 nm spectral linewidths producing ~8 μm resolution and the differentiation of different skin cells within a sample [38, 39]. A push to higher spectral bandwidths from low cost and compact semiconductor sources promises subcellular OCT resolution imaging at the point of care. Figure 1.16 plots the wavelength dependence of extinction of various constituents of biological tissue. The minima in extinction from ~1000 to ~1350 nm is termed the *biological window* and allows access to tissue over large length scales. For OCT, penetration and imaging at depths of ~2 mm is possible, and sample disturbance

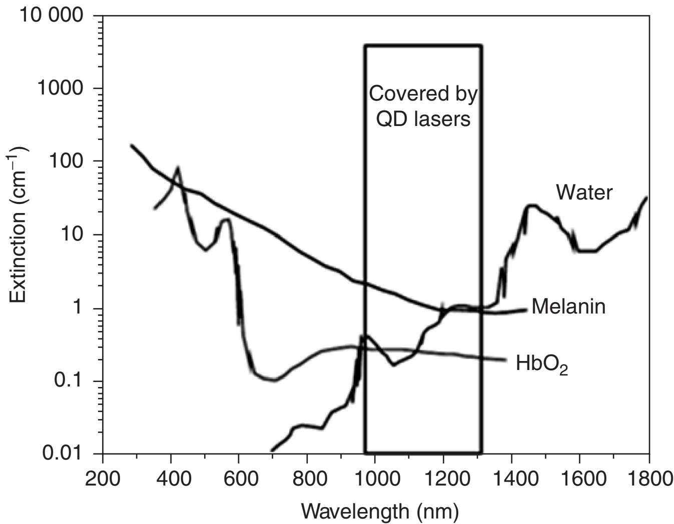

Figure 1.16 Extinction as a function of wavelength for water, melanin, and HbO_2, indicating the origin of the biological window at ~1000 to ~1350 nm.

(thermal mechanical) is minimized in nonlinear imaging. There is therefore a strong motivation to develop broad spectral bandwidth emitters and amplifiers in this spectral region. GaAs-based QD technologies allow access to this window, with conventional GaAs (<~1100 nm) and InP (>~1200 nm) QW devices operating at the limit of their wavelength ranges. A range of broadband devices including lasers, superluminescent diodes, and SOAs have been realized.

While the inhomogeneously broadened ground state and excited state emission partially overlap because of inhomogeneous broadening (Figure 1.17), when a standard "laser" active element is used as a superluminescent diode, a large modulation of the spectrum is observed owing to the very different values of gain across the emission spectrum [40]. In order to flatten the emission spectrum and obtain an emission spectrum spanning the ground and excited state emissions, the emission wavelength of the individual QD layers may be modified, typically by changing the indium composition of the QD capping layers [41, 42]. An alternate method is to vary the thickness of the capping layer while maintaining a constant indium composition [43]. In these reports, superluminescent emission of emission bandwidths of 120 nm [41], 85 nm [42], and a lasing spectrum 75 nm wide [43] were obtained. Such devices have been employed in OCT imaging of skin tissue in both time domain OCT using a superluminescent diode [38, 39] and frequency domain OCT using an SOA-based swept laser [44]. Figure 1.18 shows a 3D image obtained in the work described in Ref. [44] with a 95 nm sweep bandwidth. Identical SOAs in an optimized quasi-Littrow configuration demonstrated 202 nm tuning range and high powers [45], indicating the promise of such devices in high-resolution biomedical imaging.

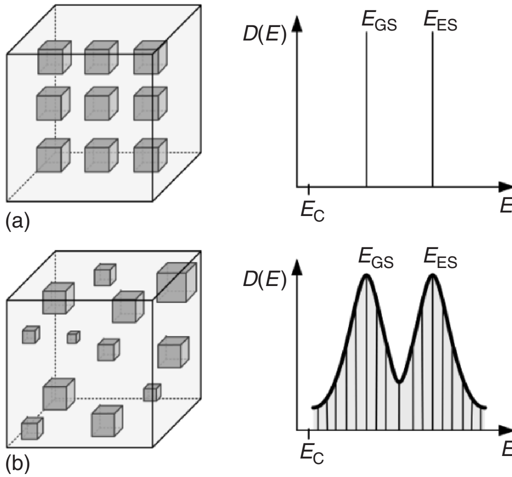

Figure 1.17 Ideal quantum dots, exhibiting perfect uniformity and resonant density of states for all electronic states and optical transitions (a). The effect of structural and compositional inhomogeneity (b) is to introduce an inhomogeneous broadening to these states and transitions.

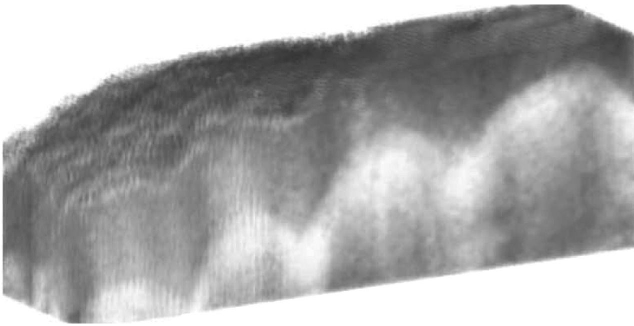

Figure 1.18 Three-dimensional skin tissue image obtained using optical coherence tomography using a quantum dot-based semiconductor optical amplifier. (Source: Krstajić *et al.* 2011 [44]. Reproduced with permission of IEEE Photonics Technol Lett.)

Further techniques continue to be employed to broaden the gain and emission spectrum of QD-based materials in this spectral region. The introduction of a QW in a hybrid QW/QD active element has led to spontaneous emission spectra >250 nm and modal gain over ~ 300 nm [46]. Primarily, the QD layers employed in these broad bandwidth devices utilize structures modified from QD laser research, with wavelength variation in the different layers in the growth direction. An alternative approach has been to revisit the growth conditions of the QDs with a view to broad spectral bandwidth applications. Here, optimization for high QD density and high inhomogeneity lead to a superluminescent diode made up of identical (yet highly inhomogeneous) layers yielding 160 nm 3 dB bandwidths with milliwatt power

levels [47]. The opportunities for further development of QD epitaxy for broadband applications is highlighted by this preliminary study [48].

In addition to the variation of the emission wavelength in the growth direction, postgrowth intermixing allows the variation of emission energy of a device along the length of its waveguide [49]. Figure 1.19a shows a schematic to highlight how such a change of emission in the plane of the optical waveguide allows new, multiplexed superluminescent diodes and SOAs to be imagined. The use of postgrowth intermixing to realize an active device is challenging, with such technologies typically being used to realize nonabsorbing mirrors in laser devices [50]. The importance of modulation p-doped materials to realize high-quality intermixed active devices has been demonstrated [51], with the p-doped materials showing less sensitivity to the intermixing process and higher quality devices for a given wavelength shift. This result suggests that selective area intermixed superluminescent devices are an exciting next step. Figure 1.19c–d shows electroluminescence results from selective area intermixed devices utilizing two and three intermixed regions, respectively. An emission spectrum of 310 nm was obtained for the latter device, which translates to a theoretical axial resolution of 2.4 μm [52].

1.4.5 Ultrafast Gain Recovery

Slow carrier relaxation in a QD structure was theoretically predicted to be a major hindrance for high luminescence efficiency and a key inhibitor for high-quality laser devices [53]. This was due to the phonon bottleneck, whereby the discrete energy levels of the QD make the energy and momentum conservation of carrier relaxation via phonon emission unlikely. As a result, it was predicted that carriers would not typically be able to relax to the lowest energy QD states within a typical carrier lifetime (∼nanoseconds) (see Figure 1.20).

However, once high optical quality structures were realized, it was apparent that strong emission was indeed observed from the lowest energy states of the QD. Time-resolved differential transmission spectroscopy allowed the carrier relaxation times to be characterized, indicating that electrons scattered (scattering time 5 ps) from holes, which in turn can relax rapidly via phonon emission (scattering time 0.6 ps) [55]. This strong carrier–carrier scattering ameliorates the phonon bottleneck. Indeed, QD structures exhibit the ultimate in ultrafast recovery time ($<$1 ps), under both gain and absorption conditions [56]. The fast absorption recovery time is especially useful for enabling saturable absorbers to mode-lock lasers at high repetition rates, where the absorption recovery should occur within the round-trip time of the cavity. Crucially, the shaping mechanism of the fast absorption recovery also enhances the shortening of the mode-locked pulses, and thus QD-based lasers have real potential for generating much shorter pulses than their QW counterparts. QD saturable absorbers also exhibit lower absorption saturation fluence than QW materials, which strongly assists the self-starting of high-frequency mode-locking [57]. Investigations of the amplification of the femtosecond pulses [54] and the ultrafast carrier dynamics of QD structures imply that such structures can be used

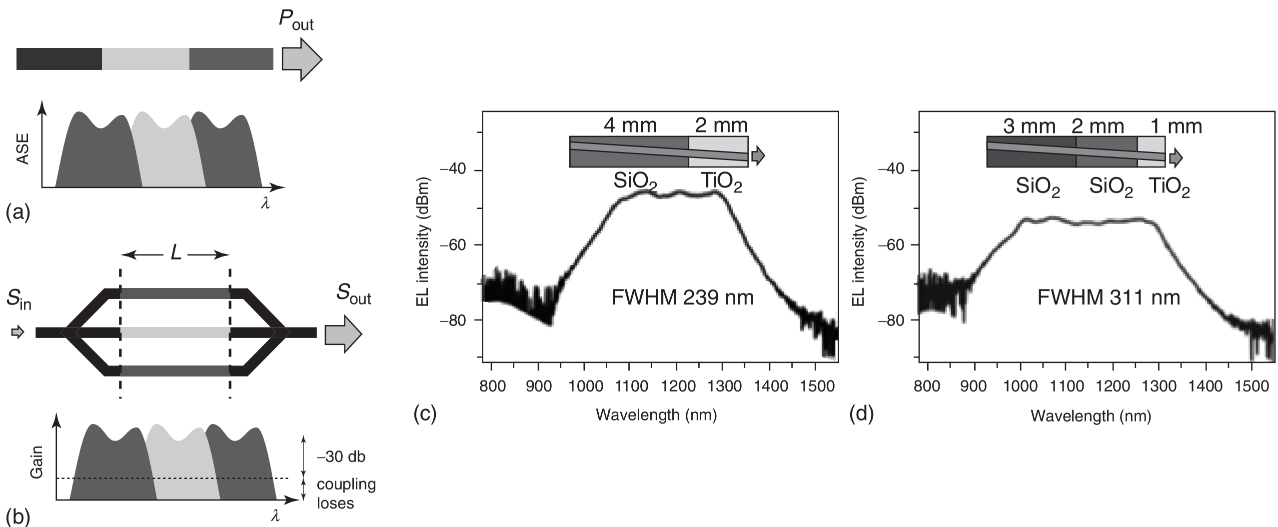

Figure 1.19 (a,b) The schematic of hybrid broadband devices with laterally or parallel integrated optical elements for superluminescent diodes, and optical amplifiers, respectively. (c,d) The schematic device structures and the corresponding electroluminescence spectra of the broadband devices with two and three laterally integrated sections. (Source: Zhou *et al*. 2012 [52]. Reproduced and modified with permission of Opt. Express.)

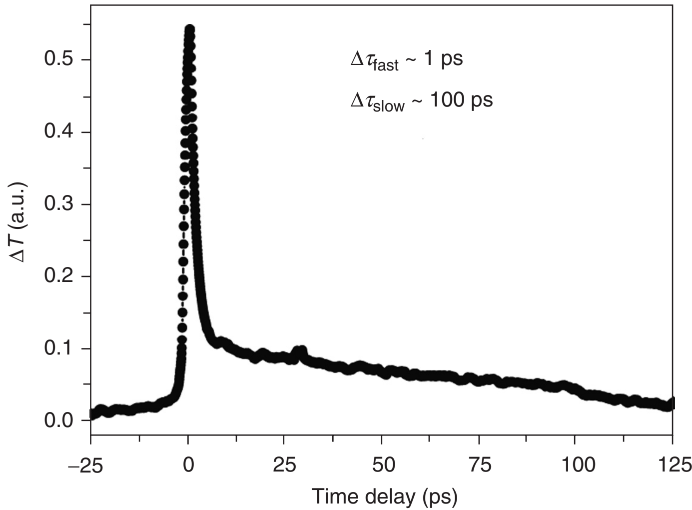

Figure 1.20 Pump–probe measurements of the carrier lifetime of a QD waveguided device. $\Delta\tau_{fast}$ and $\Delta\tau_{slow}$ are fast and slow recovery times, respectively, and ΔT corresponds to the temporal changes in transmission. (Source: Rafailov *et al.* 2003 [54]. Reproduced with permission of IEEE Photonics Technol Lett.)

simultaneously as efficient broadband gain media and as fast saturable absorbers, either independently or monolithically, and thus can have a potentially enormous impact in ultra-short-pulse laser design.

1.5 Extension of Emission Wavelength of GaAs-Based Quantum Dots

Existing QD technologies cover the near infrared (0.95–1.35 μm) wavelengths, and are a relatively mature technology. As mentioned previously, they offer wavelength coverage of special interest for biophotonic applications. However, technologies to shorter wavelengths (~0.8 μm) offer opportunities as red-emitting lasers and as passive devices for mode-locking Ti:sapphire lasers. Similarly, longer wavelength QD structures (~1.55 μm) offer opportunities as active and passive optical devices for fiber-optics communications.

1.5.1 Short-Wavelength Quantum Dot Light Emission

1.5.1.1 InP/GaInP Quantum Dots

The InP/GaAs system has around half the strain of the InAs/GaAs system. However, in order to obtain efficient carrier confinement, the choice of matrices to insert the InP QDs within is limited. In 1997, Seifert *et al.* [58] demonstrated light emission at ~0.76 μm at 5 K from an InP/InGaP QD structure. In their work, the deposition of 2.4 ML of InP on InGaP lattice matched to GaAs led to the formation

of InP QDs, while with a 3–12 s growth interruption, the deposition of 1.8 ML of InP also realized InP QDs. This behavior is similar to InAs/GaAs QDs, in which the formation of InP QDs will consume the InP wetting layer materials, as was described in Section 1.3. Following on from this work, in 2005, Smowton *et al.* [59] developed InP/InGaP QD lasers working in the 690–750 nm wavelength range. In their work, they systemically investigated the effects of the orientation of the GaAs substrate and growth conditions on the optical properties of the InP QDs. They utilized a low-pressure (150 Torr) horizontal flow MOVPE reactor with a growth temperature of 650–690 °C.

They found that the use of misorientated substrates allows for a reduction in the surface diffusion length and therefore results in the formation of small dots. This is critical for devices application because large dots will generally be associated with defects and dislocations. They obtained a QD laser device by using InP/InGaP QD structures grown on a (100) GaAs substrate misorientated 10° toward [111].

These QD materials have subsequently been utilized as semiconductor saturable absorber mirrors (SESAMs) in a Ti:sapphire laser system to realize high repetition rates (see Chapter 4). Annular dark-field (ADF) scanning transmission electron microscopy (STEM) imaging in a JEOL 2010F field-emission transmission electron microscope was employed to study the density and the size of these QDs. Figure 1.21a (where the growth direction is from bottom left to top right) shows stacks of QDs where the QDs in the lower two or three layers have a well-defined geometry while the upper ones appear flatter and laterally diffuse. The In content appears highest in the upper halves of the nominally pure InP QDs (up to $x_{In=0.8}$ was obtained from energy-dispersive X-ray mapping of the $In_xGa_{1\text{-}x}P$ alloy), indicating same intermixing at least with the lower barriers. Also, in some areas, such as near the top of the figure (Figure 1.21b), cation ordering on alternating {111} lattice planes is visible, pointing to the onset of spinodal decomposition in the ternary GaInP alloy of the barrier. These structures showed strong PL at 775 nm and were successfully incorporated into $Al_{0.2}Ga_{0.8}As$/AlAs-based SESAMs [60].

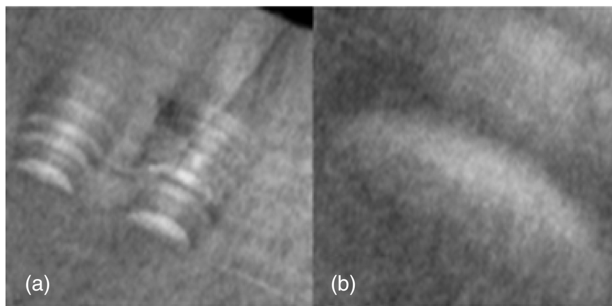

Figure 1.21 (a) InP QDs at 250-k× magnification in ADF mode and (b) ADF lattice images of QDs at 1.2-M× magnification. (Source: Butkus *et al.* 2011 [60]. Reproduced with permission of IEEE Photonics Technol Lett.)

1.5.1.2 Type II InAlAs/AlGaAs Quantum Dots

The quantum-confinement-induced type I to type II transition in GaAs/AlGaAs QDs was theoretically predicted in 1996 [61]. In the GaAs/AlGaAs QD system, if the GaAs QDs are very small, quantum confinement effects will enable the valley of the conduction band of GaAs to exceed the valley of the conduction band of AlGaAs, resulting in indirect type II optical transitions. In this case, holes and electrons are spatially separated, with the hole being localized in the QDs and the electrons being localized in the barrier via Coulomb attraction. However, owing to the very small lattice mismatch between GaAs and AlGaAs, the related GaAs/AlGaAs QDs are very difficult to realize.

However, GaAs-based InAlAs/AlGaAs QDs [62–64] have been realized, making the experimental observation of transformation from type I to type II optical transition possible. In reality, besides fundamental physical studies, InAlAs/AlGaAs QDs have great potential to fabricate short-wavelength QD materials and devices. Figure 1.22 shows a schematic bandgap diagram of type I and type II InAlAs/AlGaAs QDs. Power-dependent and temperature-dependent PL experiments can be used to discriminate the type I and type II optical transitions from dots of different sizes. Generally, for type II InAlAs/AlGaAs QDs, the emission peak is blueshift with increasing the pumping power, and there are higher order transitions appearing with increasing temperature. The growth temperature is a key parameter for achieving high-quality InAlAs/AlGaAs QD structures. As described in Section 1.3, an appropriately high growth temperature will increase the migration length of aluminum atoms, thereby reducing the incorporation of impurities and group III vacancies.

1.5.2 Long-Wavelength QD Light Emission

For a range of reasons, such as the availability of high refractive index contrast of materials, advantageous band offsets, and high thermal conductivity, GaAs-based QDs offer significant promise for fiber-optics communication applications if they could be realized at 1.55 μm. The ability to realize high-quality distributed Bragg reflectors (DBRs) and high-quality QD materials is of particular advantage for

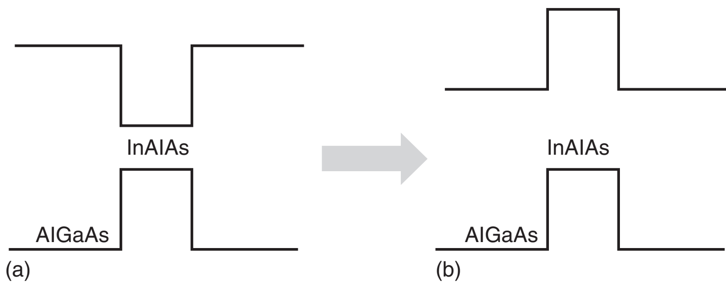

Figure 1.22 Schematic bandgap diagram of (a) type I and (b) type II InAlAs/AlGaAs quantum dots.

mode-locking applications. As a result, for over 10 years, people have made great efforts in extending the emission wavelength to the 1.55 μm range. However, it is extremely difficult to shift the emission wavelength of GaAs-based QDs to 1.55 μm. This is due to the need for large QDs with high indium composition in its capping layer, which may easily induce a large (debilitating) number of defects and dislocations [65]. Here, we describe the techniques that have been previously employed and discuss epitaxial techniques recently developed to obtain 1550 nm GaAs-based QDs.

1.5.2.1 Low Growth Temperature InAs/GaAs Quantum Dots

In 1999, Maximov *et al*. obtained 1.75 μm light emission from InAs/GaAs QD cluster, which were grown at a very low temperature of ∼320–400 °C. These are actually a kind of laterally coupled InAs QDs formed on a GaAs layer, which are quite different from typical QDs [66].

1.5.2.2 InAs QDs Grown on an InGaAs Metamorphic Layer

In 2003, Ledentsov *et al*. [67] realized InAs QDs on a thick $In_{0.2}Ga_{0.8}As$ metamorphic layer, and realized a 1.5 μm broad area laser, which simultaneously demonstrated a high differential efficiency of 50%, a low threshold current density, and a high operating temperature of >80 °C.

1.5.2.3 InGaAsSb Capped InAs/GaAs Quantum Dots and InGaNAs Capped InAs/GaAs Quantum Dots

In 2005, Ripalda *et al*. [68] obtained 1.6 μm light emission from InGaAs QDs capped by 8 nm GaAsSb layer structure. Compared to GaAs-capped InGaAs QD samples, a large redshift in the emission wavelength is attributed to the move to a type II optical transition from the QD materials. In 2006, Richter *et al*. [69], utilized a quaternary $In_{0.15}Ga_{0.85}As_{1-x}N_x$ layer to cap InAs QDs, and obtained 1.5 μm light emission. It was found that the annealing process could help enhance the optical quality of the QDs, with the optimum annealing temperature being closely related to the nitrogen composition.

1.5.2.4 Bilayer InAs/GaAs QD Structures

In 2011, by using a bilayer QD structure with a small InAs QD layer and a large InAs QD layer closely stacked, room temperature electroluminescence emission at 1.52 μm and lasing at 1.42 μm were obtained. This is due to strongly modified strain distribution in the upper QD layer by the seed QD layer, allowing the realization of large dislocation-free QDs. This allows a significant extension of the room temperature light emission wavelength [70]. Figure 1.23 shows a GaAs-capped bilayer QD structure and an InGaAs-capped bilayer QD structure.

1.5.2.5 Asymmetric Dot in WELL QD Structure

Compared to the development of 1.3 μm GaAs-based QDs, the shift to 1.55 μm poses significant challenges in materials science and engineering. Following the introduction of a strained InGaAs cap layer to reach 1.3 μm, pushing the technology

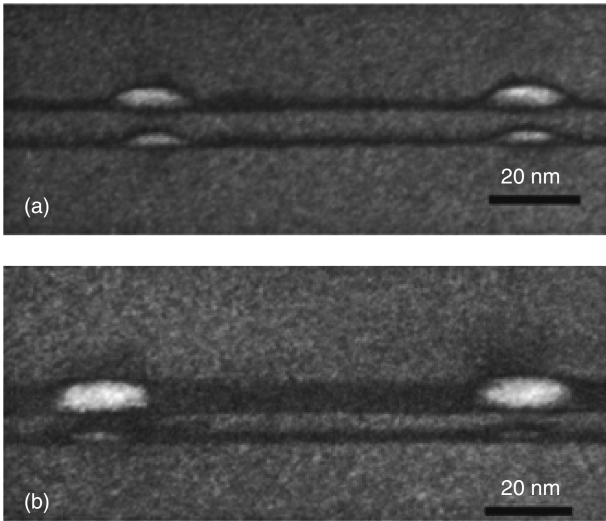

Figure 1.23 Cross-sectional TEM images of bilayer InAs/GaAs QD structures (a) with GaAs capping layer and (b) with InGaAs capping layer of the upper, emitting quantum dot layer. (Source: Majid *et al*. 2011 [70]. Reproduced with permission of IEEE J. Sel. Top. Quantum Electron.)

to 1.55 μm devices would logically require even higher indium content QD capping layers. However, until now there are only a few studies in this direction [71, 72]. High indium concentration in the QDs and the surrounding matrix very readily induces nonradiative recombination centers that rapidly degrade the crystal and optical quality of the QDs, making such QD materials unsuitable for device applications. Alternative methods to ameliorate this issue are capping InAs/GaAs QDs with quaternary InGaNAs [69] or InGaAsSb [68] layers, which significantly complicates the epitaxial growth process and is detrimental to the optical and material qualities of the QDs. Emission around 1.5 μm has also been obtained from an InAs/GaAs QD structure grown on thick metamorphic InGaAs buffer layers/virtual substrates [67], but repeatability and reliability are significant issues for such structures, as is the difficulty in growing thick lattice-matched alloys or DBRs. The development of high-quality 1.55 μm QDs, compatible with other GaAs technologies (e.g., DBRs, photonic crystals), remains a key goal for QD epitaxy research.

To mitigate the difficulties outlined above, we developed the epitaxy process for an asymmetric InGaAs/GaAs dot-in-well (DWELL) structure with room temperature photoluminescence (RT-PL) at 1.55 μm comparable to that of 1.3 μm QD structures. Such structures were used to fabricate a quantum dot-saturable absorber mirror (QD-SAM) in this spectral regime. The QD-SAMs were designed for mode-locking a 10 GHz pulse repetition rate Er-doped laser generating 2.4 ps pulses at 1.55 μm central wavelength. Detailed description on this QD technology can be found in Chapter 4.

1.6 Future Prospects

The following chapters in this book detail the development of a range of new optoelectronic devices, ultrafast lasers, and their use in a range of applications. In the short term, the continued development of these emerging device applications will drive materials optimization for these devices. Increase and control of QD areal density and control of inhomogeneous broadening (both highly homogeneous *and* inhomogeneous) remain key areas of materials development.

In the longer term, we can expect the development of materials at shorter and longer wavelengths. For shorter wavelengths, SESAM devices at wavelengths optimal for Ti:sapphire lasers offer routes to higher repetition rate mode-locked lasers, as discussed in Chapter 4 [60]. Following on from this work, and excellent results from QD-based optically pumped vertical external cavity surface emitting lasers (OP-VECSELs) as described in Chapter Y, the development of QD-based electrically pumped vertical external cavity surface emitting lasers (EP-VECSELs) at wavelengths of ~650–900 nm can be easily imagined. The development of shorter wavelength, high-quality GaAs-based QDs is nontrivial. Furthermore, the intermediate wavelength range (~900 nm) poses a ''gap'' due to the choice of materials (InP/GaInP, InGaAs/(Al)GaAs). The differing band offsets, thermal barriers to carrier escape, and reliability issues with aluminum-containing active elements, all make the identification of the best QD technologies unclear. The applications in biophotonics/biomedical sciences are strong. While the Ti:sapphire is a workhorse in many research laboratories worldwide, its optimization in terms of repetition rate and pulse characteristics is important. Moreover, the replacement of the Ti:sapphire laser with an all-semiconductor device holds significant potential for widespread use in emerging imaging/therapy/surgical applications.

For longer wavelengths, while 10 GHz QD SESAM mode-locked lasers have been recently demonstrated [65], the optimization of such devices offers opportunities for higher repetition-rate mode-locked lasers, and can be expected to be an active research area over the coming years. Following on from this, active elements based on this technology offer exciting prospects. While achieving characteristics suitable for device performance to challenge InP-based devices (i.e., high modal gain, high differential gain, high characteristic temperature) will be challenging, broad spectral bandwidths and the integration of such technologies with DBRs for vertical devices (e.g., SESAMs) and air-bridge photonic crystal devices [73] offers new routes to realize high-speed switching devices. The reduction influence required to saturate absorption, the low volume, and high speed of gain/absorption recovery may place these materials as being highly important for all-optical signal processing applications [74].

The development of ultra-broad spectral bandwidth sources may be a killer application for QD-based devices [45], assisted by the control of inhomogeneity of QDs [70]. Intermixing [52] for postgrowth control of the emission wavelength over the longitudinal direction of a waveguide device poses some interesting opportunities for advanced devices. In particular, enabling active intermixed devices

that may be coupled to the excited state of regions of the wafer where intermixing is inhibited may combine benefits of mode-locking using the excited state, yet lasing from the lower current density ground state.

In addition, the incorporation of QWs along with multiQD active elements poses significant promise. Future work on the use of multiple "chirped" QWs can be expected to produce even greater spectral bandwidths. In addition, the use of both shorter wavelength (InGaAs) and longer wavelength (InGaAsN, InGaAsSb) QWs may extend the spectral coverage of GaAs-based devices. It is important to point out that this type of active element has yet to be applied to the full range of QD systems such as short-wavelength InP/InGaP (GaAs substrate) and InAs/InGaAsP (InP substrate). The application of additional QW elements may impact upon enhancing spectral bandwidth coverage for these materials systems.

Acknowledgments

The authors would like to acknowledge the support from the EU FP7 FAST-DOT (224338). We gratefully acknowledge Igor Krestnikov from Innolume GmbH for the MBE growth.

References

1. Quist, T.M., Rediker, R.H., Keyes, R.J., Krag, W.E., Lax, B., McWhorter, A.L., and Zeigler, H.J. (1962) Semiconductor laser of GaAs. *Appl. Phys. Lett.*, **1**, 91–92.
2. Arakawa, Y. and Sakaki, H. (1982) Multidimensional quantum well laser and temperature-dependence of its threshold current. *Appl. Phys. Lett.*, **40**, 939–941.
3. Asada, M., Miyamoto, Y., and Suematsu, Y. (1986) Gain and the threshold of three-dimensional quantum-box lasers. *IEEE J. Quantum Electron.*, **QE-22**, 1915.
4. Alexander, R.R., Agarwal, H., Groom, K.M., Liu, H., Hopkinson, M., Hogg, R.A., Ishida, M., Yamamoto, T., Sugawara, M., and Arakawa, Y. (2007) Systematic study of the effects of δ-p-doping on 1.3 μm quantum dot lasers. *IEEE J. Q. Electron.*, **43**, 1129–1140.
5. Vahala, K.J. (1988) Quantum box fabrication tolerance and size limits in semiconductors and their effect on optical gain. *IEEE J. Quantum Electron.*, **QE-24**, 523.
6. Clausen, E.M. Jr.,, Craighead, H.G., Warlock, J.M., Harbison, J.P., Schiavone, L.M., Florez, L., and Van dar Gaag, B. (1989) Determination of nonradiative surface layer thickness In quantum dots etched from single quantum wen GaAsl AlGaAs. *Appl. Phys. Lett.*, **55**, 1427.
7. Hirayama, H., Matsunaga, K., Asada, M., and Suematsu, Y. (1994) Lasing action of $Ga_{0.67}ln_{o.33}As$/GalnAsP/lnP tensile-strained quantum-box laser. *Electron Lett.*, **30**, 142.
8. Ishida, S., Arakawa, Y., and Wada, K. (1998) Seeded self-assembled GaAs quantum dots grown in two-dimensional V grooves by selective metal–organic chemical-vapor deposition. *Appl. Phys. Lett.*, **72**, 800.
9. Gibbon, M., Stagg, J.P., Cureton, C.G., Thrush, E.J., Jones, C.J., Mallard, R.E., Pritchard, R.E., Collis, N., and Chew, A. (1993) Selective-area low-pressure MOCVD of GaInAsP and related materials on planar InP substrates. *Semicond. Sci. Technol.*, **8**, 998–1010.
10. Brandt, O., Tapfer, L., Ploog, K., Bierwolf, R., Hohenstein, M., Phillipp, F., Lage, H., and Heberle, A. (1991) InAs quantum dots in a single-crystal GaAs matrix. *Phys. Rev. B*, **44**, 8043.

11. QDLASER, Inc and Innolume GmbH *www.qdlaser.com*, and *www.innolume.com* (accessed 17 June 2013).
12. Cho, A.Y. and Arthur, J.R. (1975) in *Progress in Solid State Chemistry*, (eds G.A. Somorjai and J.O. McCaldin), Pergamon, Oxford, Vol. 10, p. 157.
13. EPSRC *http://www.epsrciii-vcentre.com/Home.aspx* (accessed 16 June 2013).
14. Gerard, M., Genin, J.B., Lefebvre, J., Moison, J.M., Lebouche, N., and Barthe, F. (1995) Optical investigation of the self-organized growth of InAs/GaAs quantum boxes. *J. Crystal. Growth*, **150**, 351.
15. Ratsch, C. and Zangwill, A. (1993) Equilibrium theory of the Stranski-Krastanov epitaxial morphology. *Surf. Sci.*, **293**, 123.
16. Priester, C. and Lannoo, M. (1995) Origin of self-assembled quantum dots in highly mismatched heteroepitaxy. *Phys. Rev. Lett.*, **75**, 93.
17. Garcia, J.M., Medeiros-riberiro, G., Schmidt, K., Ngo, T., Feng, J.L., Lorke, A., Kotthaus, J., and Petroff, P.M. (1997) Intermixing and shape changes during the formation of InAs self-assembled quantum dots. *Appl. Phys. Lett.*, **71**, 2014.
18. Tersoff, J. (1998) Enhanced nucleation and enrichment of strained-alloy quantum dots. *Phys. Rev. Lett.*, **81**, 3183.
19. Meng, X.Q., Jin, P., Liang, Z.M., Liu, F.Q., Wang, Z.G., and Zhang, Z.Y. (2010) Structure and properties of InAs/AlAs quantum dots for broadband emission. *J.Appl. Phys.*, **108**, 103515.
20. Ledentsov, N.N., Shchukin, V.A., Grundmann, M., Kirstaedter, N., Böhrer, J., Schmidt, O., Bimberg, D., Ustinov, V.M., Egorov, A.Y., Zhukov, A.E., Kop'ev, P.S., Zaitsev, S.V., Yu, N., Gordeev, Z., Alferov, I., Borovkov, A.I., Kosogov, A.O., Ruvimov, S.S., Werner, P., Gösele, U., and Heydenreich, J. (1996) Direct formation of vertically coupled quantum dots in Stranski-Krastanow growth. *Phys. Rev. B*, **54**, 8743.
21. Leonard, D., Krishnamurthy, M., Reaves, C.M., Denbaars, S.P., and Petroff, P.M. (1993) Direct formation of quantum-sized dots from uniform coherent islands of InGaAs on GaAs surfaces. *Appl. Phys. Lett.*, **63**, 3203.
22. Yamaguchi, K., Yujobo, K., and Kaizu, T. (2000) Stranski-Krastanov growth of InAs quantum dots with narrow size distribution. *Jpn. J. Appl. Phys.*, **39**, 1245.
23. Liu, H.Y., Zhou, W., Ding, D., Jiang, W.H., Xu, B., Liang, J.B., and Wang, Z.G. (2000) Self-organized type-II $In_{0.55}Al_{0.45}As/Al_{0.50}Ga_{0.50}As$ quantum dots realized on GaAs (311)A. *Appl. Phys. Lett.*, **76**, 3741.
24. Chu, L., Arzberger, M., Böhm, G., and Abstreiter, G. (1999) Influence of growth conditions on the photoluminescence of self-assembled InAs/GaAs quantum dots. *J. Appl. Phys.*, **85**, 2355.
25. Seifert, W., Carlsson, N., Johansson, J., Pistol, M.-E., and Samuelson, L. (1997) In situ growth of nano-structures by metal-organic vapour phase epitaxy. *J. Crystal. Growth*, **170**, 39–46.
26. Shchukin, V.A., Ledenstov, N.N., Kop'ev, P.S., and Bimberg, D. (1995) Spontaneous ordering of arrays of coherent strained islands. *Phys. Rev. Lett.*, **75**, 2968.
27. Marko, I.P., Massé, N.F., Sweeney, S.J., Andreev, A.D., Adams, A.R., Hatori, N., and Sugawara, M. (2005) Carrier transport and recombination in p-doped and intrinsic 1.3 μm InAs/GaAs quantum-dot lasers, **87**, 211114.
28. Otsubo, K., Hatori, N., Ishida, M., Okumura, S., Akiyama, T., Nakata, Y., Ebe, H., Sugawara, M., and Arakawa, Y. (2004) Temperature-insensitive eye-opening under 10-Gb/s modulation of 1.3-_m P-doped quantum-dot lasers without current adjustments. *Jpn. J. Appl. Phys.*, **43** (8B), L1124–L1126.
29. Fathpour, S., Mi, Z., Bhattacharya, P., Kovsh, A.R., Mikhrin, S.S., Krestnikov, I.L., Kozhukhov, A.V., and Ledentsov, N.N. (2004) The role of Auger recombination in the temperature-dependent output characteristics ($T_0 = \infty$) of p-doped 1.3 μm quantum dot lasers. *Appl. Phys. Lett.*, **85**, 5164.
30. Ozgur, G., Demir, A., and Deppe, D.G. (2009) Threshold temperature dependence of a quantum-dot laser diode with

and without p-doping. *IEEE J. Quantum Electron.*, **45** (10), 1265, and references therein..

31. Bimberg, D. (2005) Quantum dot for lasers, amplifiers and computing. *J. Phys. D. Appl. Phys.*, **38**, 2005.
32. Kirstaedter, N., Ledentsov, N.N., Grundmann, M., Bimberg, D., Ustinov, V.M., Ruvimov, S.S., Maximov, M.V., Kop'ev, P.S., Alferov, Z.I., Richter, U., Werner, P., Goesele, U., and Heydenreich, J. (1994) Low-threshold, large to injection-laser emission from (InGa)As quantum dots. *Electron. Lett.*, **30**, 1416–1418.
33. Liu, H.Y., Sellers, I.R., Badcock, T.J., Mowbray, D.J., Skolnick, M.S., Groom, K.M., Gutiérrez, M., Hopkinson, M., Ng, J.S., David, J.P.R., and Beanland, R. (2004) Improved performance of 1.3 μm multilayer InAs quantum-dot lasers using a high-growth-temperature GaAs spacer layer. *Appl. Phys. Lett.*, **85**, 704.
34. Salhi, A., Martiradonna, L., Visimberga, G., Tasco, V., Fortunato, L., Todaro, M.T., Cingolani, R., Passaseo, A., and De Vittorio, M. (2006) High-Modal Gain 1300-nm In(Ga)As–GaAs quantum-Dot Lasers. *IEEE Photonics Technol. Lett.*, **18** (16), 1735.
35. Sugawara, M., Mukai, K., Nakata, Y., Ishikawa, H., and Sakamoto, A. (2000) Effect of homogeneous broadening of optical gain on lasing spectra in self-assembled $In_xGa_{1-x}As$/GaAs quantum dot lasers. *Phys. Rev. B*, **61**, 7595–7603.
36. Rafailov, E.U., Cataluna, M.A., and Sibbett, W. (2007) Mode-locked quantum-dot lasers 2. *Nat. Photonics*, **1**, 395–401.
37. Drexler, W. (2004) Ultrahigh resolution optical coherence tomography. *J. Biomed. Opt.*, **9**, 47–74.
38. Greenwood, P.D.L., Childs, D.T.D., Kennedy, K., Groom, K.M., Hugues, M., Hopkinson, M., Hogg, R.A., Krstajić, N., Smith, L.E., Matcher, S.J., Bonesi, M., Macneil, S., and Smallwood, R. (2010) Quantum dot superluminescent diodes for optical coherence tomography: device engineering. *IEEE J. Sel. Top. Quantum Electron.*, **16**, 1015–1022.
39. Krstajić, N., Smith, L.E., Matcher, S.J., Childs, D.T.D., Bonesi, M., Greenwood, P.D.L., Hugues, M., Kennedy, K., Hopkinson, M., Groom, K.M., MacNeil, S., Hogg, R.A., and Smallwood, R. (2010) Quantum dot superluminescent diodes for optical coherence tomography: skin imaging. *IEEE J. Sel. Top. Quantum Electron.*, **16**, 748–754.
40. Rossetti, M., Markus, A., Fiore, A., Occhi, L., and Velez, C. (2005) Quantum dot superluminescent diodes emitting at 1.3 μm. *IEEE Photonics Technol. Lett.*, **17**, 540–542.
41. Li, L.H., Rossetti, M., Fiore, A., Occhi, L., and Velez, C. (2005) Wide emission spectrum from superluminescent diodes with chirped quantum dot multilayer. *Electron. Lett.*, **41**, 41–43.
42. Ray, S.K., Groom, K.M., Beattie, M.D., Liu, H.Y., Hopkinson, M., and Hogg, R.A. (2006) Broad-band superluminescent light-emitting diodes incorporating quantum dots in compositionally modulated quantum wells. *IEEE Photonics Technol. Lett.*, **18**, 58–60.
43. Kovsh, A., Krestnikov, I., Livshits, D., Mikhrin, S., and Weimert, J. (2007) Quantum dot laser with 75 nm broad spectrum of emission. *Opt. Lett.*, **32**, 793.
44. Krstajić, N., Childs, D.T.D., Matcher, S.J., Livshits, D.A., Shkolnik, A., Krestnikov, I.L., and Hogg, R.A. (2011) Swept-source laser based on quantum-dot semiconductor optical amplifier – applications in optical coherence tomography. *IEEE Photonics Technol. Lett.*, **23**, 739.
45. Fedorova, K.A., Cataluna, M.A., Krestnikov, I.L., Livshits, D.A., and Rafailov, E.U. (2010) Broadly tunable high-power InAs/GaAs quantum-dot external cavity diode lasers. *Opt. Express*, **18**, 19438–19443.
46. Chen, S.M., Zhou, K.J., Zhang, Z.Y., Childs, D.T., and Hogg, R.A. (2012) Ultra-broadband emission form a hybrid QW/QD structure. *Appl. Phys. Lett.*, **100**, 041118-1–041118-3.
47. Majid, M.A., Hugues, M., Childs, D.T.D., and Hogg, R.A. (2012) Optimization of quantum-dot molecular beam epitaxy for broad spectral bandwidth devices. *IEEE Photonics J.*, **4**, 2066.

48. Zhang, Z.Y., Hogg, R.A., Lv, X.Q., and Wang, Z.G. (2010) Self-assembled quantum-dot superluminescent light emitting diodes. *Adv. Opt. Photon.*, **2**, 201–228.
49. Zhang, Z.Y., Jiang, Q., Hopkinson, M., and Hogg, R.A. (2010) Effects of intermixing on modulation p-doped quantum dot superluminescent light emitting diodes. *Opt. Express*, **18**, 7055–7063.
50. Walker, C.L., Bryce, A.C., and Marsh, J.H. (2002) Non absorbing mirror laser with improved catastrophic optical damage level. The 15th Annual Meeting of the IEEE Lasers and Electro-Optics Society, 2002. LEOS 2001, Vol. 2, pp. 643–644.
51. Jiang, Q., Zhang, Z.Y., Hopkinson, M., and Hogg, R.A. (2010) High performance intermixed p-doped quantum dot superluminescent diodes at 1.2 μm. *Electron. Lett.*, **46**, 295–296.
52. Zhou, K.J., Jiang, Q., Zhang, Z.Y., Liu, H.Y., Chen, S.M., and Hogg, R.A. (2012) Quantum dot selective area intermixing for broadband light sources. *Opt. Express*, **20**, 26950.
53. Benisty, H., Sotomayor-Torres, C.M., and Weisbuch, C. (1991) *Phys. Rev. B*, **44**, 10945.
54. Rafailov, E.U., Loza-Alvarez, P., Sibbett, W., Sokolovskii, G.S., Livshits, D.A., Zhukov, A.E., and Ustinov, V.M. (2003) Amplification of femtosecond pulses over by 18 dB in a quantum-dot semiconductor optical amplifier. *IEEE Photonics Technol. Lett.*, **15**, 1023–1025.
55. Sosnowski, T.S., Ann Arbor, T.B., Jiang, H., Singh, J., Kamath, K., and Bhattacharya, P. (1998) Rapid carrier relaxation in $In_{0.4}Ga_{0.6}As/GaAs$ quantum dots characterized by differential transmission spectroscopy. *Phys. Rev. B*, **57**, 9423–9426.
56. Borri, P., Langbein, W., Hvam, J.M., Heinrichsdorff, F., Mao, M.-H., and Bimberg, D. (2000) Ultrafast gain dynamics in InAs–InGaAs quantum-dot amplifiers. *IEEE Photonics Technol. Lett.*, **12**, 594.
57. Rafailov, E.U., White, S.J., Lagatsky, A.A., Miller, A., Sibbett, W., Livshits, D.A., Zhukov, A.E., and Ustinov, V.M. (2004) Fast quantum-dot saturable absorber for passive mode-locking of solid-state lasers. *IEEE Photonics Technol. Lett.*, **16**, 2439–2441.
58. Seifert, W., Carlsson, N., Johansson, J., Pistol, M.-E., and Samuelson, L. (1997) In situ growth of nano-structures by metal-organic vapour phase epitaxy. *J. Cryst. Growth*, **170**, 39.
59. Smowton, P.M., Lutti, J., Lewis, G.M., Krysa, A.B., Roberts, J.S., and Houston, P.A. (2005) InP–GaInP quantum-dot lasers emitting between 690–750 nm. *IEEE J. Sel. Top. Quantum Electron.*, **11**, 1035.
60. Butkus, M., Robertson, G., Maker, G., Malcolm, G., Hamilton, C., Krysa, A.B., Stevens, B.J., Hogg, R.A., Qiu, Y., Walther, T., and Rafailov, E.U. (2011) High repetition rate Ti: sapphire laser mode-locked by InP quantum-dot saturable absorber. *IEEE Photonics Technol. Lett.*, **23**, 1603–1605.
61. Sun, C.-K., Wang, G., Bowers, J.E., Brar, B., Blank, H.-R., Kroemer, H., and Pilkuhn, M.H. (1996) Optical investigations of the dynamic behavior of GaSb/GaAs quantum dots. *Appl. Phys. Lett.*, **68**, 1543.
62. Leon, R., Petroff, P.M., Leonard, D., and Fafard, S. (1996) Spatially resolved visible luminescence of self-assembled semiconductor quantum dots. *Science*, **274**, 1350.
63. Franceschetti, A. and Zunger, A. (1995) Quantum-confinement-induced $\Gamma \rightarrow X$ transition in GaAs/AlGaAs quantum films, wires, and dots. *Phys. Rev. B*, **52**, 14664.
64. Zhou, W., Zhu, Z.M., Liu, F.Q., Xu, B., Xu, H.Z., and Wang, Z.G. (1999) Substrate surface atomic structure influence on the growth of InAlAs quantum dots. *J. Cryst. Growth*, **608**, 200.
65. Zhang, Z.Y., Oehler, A.E.H., Resan, B., Kurmulis, S., Zhou, K.J., Wang, Q., Mangold, M., Suedmeyer, T., Keller, U., Weingarten, K.J., and Hogg, R.A. (2012) 1.55 μm InAs/GaAs quantum dots and high repetition rate quantum dot SESAM mode-locked laser. *Sci. Rep.*, **2**, 477.
66. Zhukov, A.E., Kovsh, A.R., Bert, N.A., Ustinov, V.M., Kop'ev, P.S., Alferov, Z.I., Ledentsov, N.N., Bimberg, D.,

Soshnikov, I.P., and Werner, P. (1999) Optical and structural properties of InAs quantum dots in a GaAs matrix for a spectral range up to 1.7 μm. *Appl. Phys. Lett.*, **75**, 2347.

67. Ledentsov, N.N., Kovsh, A.R., Zhukov, A.E., Maleev, N.A., Mikhrin, S.S., Vasil'ev, A.P., Semenova, E.S., Maximov, M.V., Shemyakov, Y.M., Kryzhanovskaya, N.V., Ustinov, V.M., and Bimberg, D. (2003) High performance quantum dot lasers on GaAs substrates operating in 1.5 pm range. *Electron Lett.*, **39**, 1126.

68. Ripalda, J.M., Ripalda, D., Granados, Y., González, A.M., Sánchez, S.I., and Molina, J.M. (2005) García room temperature emission at 1.6 mu m from InGaAs quantum dots capped with GaAsSb. *Appl. Phys. Lett.*, **87**, 202108.

69. Richter, M., Damilano, B., Massies, J., Duboz, J.Y., and Wieck, A.D. (2006) $InAs/In_{0.15}Ga_{0.85}As_{1-x}N_x$ quantum dots for 1.5 mu m laser applications. *Prog. Semicond. Mater. V: Novel Mater. Electron. Optoelectron. Appl.*, **891**, 185–190.

70. Majid, M.A., Childs, D.T.D., Shahid, H., Chen, S., Kennedy, K., Airey, R.J., Hogg, R.A., Clarke, E., Howe, P., Spencer, P.D., and Murray, R. (2011) Toward 1550-nm GaAs-based lasers using InAs/GaAs quantum dot bilayers. *IEEE J. Sel. Top. Quantum Electron.*, **17**, 1334.

71. Seravalli, L., Frigeri, P., Trevisi, G., and Franchi, S. (2008) 1.59 μm room temperature emission from metamorphic InAs/InGaAs quantum dots grown on GaAs substrates. *Appl. Phys. Lett.*, **92**, 213104.

72. Tatebayashi, J., Nishioka, M., and Arakawa, Y. (2001) Over 1.5 μm light emission from InAs quantum dots embedded in InGaAs strain-reducing layer grown by metalorganic chemical vapor deposition. *Appl. Phys. Lett.*, **78**, 3469–3471.

73. Asakawa, K., Sugimoto, Y., Watanabe, Y., Ozaki, N., Mizutani, A., Takata, Y., Kitagawa, Y., Ishikawa, H., Ikeda, N., Awazu, K., Wang, X., Watanabe, A., Nakamura, S., Ohkouchi, S., Inoue, K., Kristensen, M., Sigmund, O., Borel, P.I., and Baets, R. (2006) Photonic crystal and quantum dot technologies for all-optical switch and logic device. *New J. Phys.*, **8**, 208.

74. Wada, O. (2011) Recent progress in semiconductor-based photonic signal-processing devices. *IEEE J. Sel. Top. Quantum Electron.*, **17** (2), 309.